Front. Chem. Sci. Eng. 2021, 15(4): 820–836
https://doi.org/10.1007/s11705-020-1997-7

REVIEW ARTICLE

# Recent progress in the design and fabrication of MXene-based membranes

**Kai Qu**[1], **Kang Huang** (✉)[2], **Zhi Xu** (✉)[1]

1 State Key Laboratory of Chemical Engineering, School of Chemical Engineering, East China University of Science and Technology, Shanghai 200237, China
2 State Key Laboratory of Materials-Oriented Chemical Engineering, College of Chemical Engineering, Nanjing Tech University, Nanjing 211816, China



**Abstract** Two-dimensional membranes have attracted significant attention due to their superior characteristics, and their ability to boost both flux and selectivity have led to their reputation as potential next-generation separation membranes. Among them, emerging MXene-based membranes play significant roles in the competitive membrane-separation field. In this mini-review, we systematically discuss the assembly and separation mechanisms of these membranes. Moreover, we highlight strategies based on the crosslinking of MXene nanosheets and the construction of additional nanochannels that further enhance the permeabilities and anti-swelling properties of MXene-based membranes and meet the requirements of practical applications, such as gas-molecule sieving, ion sieving, and other small-molecule sieving. MXene nanosheets can also be used as additives that introduce specific functionalities into hybrid membranes. In addition, extended applications that use MXenes as scaffolds are also discussed.

**Keywords** MXene, 2D materials, membranes, separation

## 1 Introduction

Since graphene was discovered in 2004, various two-dimensional (2D) materials have attracted significant levels of attention and have been extensively studied in many fields. Their unique physicochemical properties are attractive for energy-storage, sensor, supercapacitor, catalysis, and optoelectronics applications [1–5]. In particular, the readily tunable physicochemical properties and distinct laminar structures of 2D materials make them competitive materials for use in membrane-separation applications, such as gas-molecule sieving [6–12], ion sieving [13–18], dye rejection [19–25], and solvent dehydration [26–28]. For example, laminar graphene oxide (GO) membranes have been intensively investigated for small-molecule sieving by adjusting interlayer spacings to suitable values. Kim et al. [29] prepared ultrathin (3–10 nm) GO membranes using various stacking methods. Selective gas diffusion in a GO membrane is readily achieved by tuning the gas flow channels and pores, as demonstrated by the desirable gas-molecule sieving characteristics of GO. Moreover, the interlayer spacing of a GO membrane in water can be controlled to a precision of 1 Å by intercalating one kind of ion, thereby enabling corresponding ions to be sieved [13].

Recently, MXenes, as a new class of 2D material discovered by Naguib et al. [30,31], have been widely explored as their structures are remarkably similar to that of GO [3,30]. Usually, MXenes are prepared by selectively etching the *sp*-element layers from the corresponding MAX ($M_{n+1}AX_n$, $n$ = 1, 2, 3) precursor phase, where M is a transition metal (Ti, Sc, V, etc.), A is a main-group *sp* element (Cd, Al, Si, etc.), and X is C or N [31,32]. The MXene produced in this manner has the formula $M_{n+1}X_nT_x$ ($n$ = 1, 2, 3), where $n$ determines the thickness of the MXene, T represents surface functional groups, such as oxygen (= O), hydroxyl (–OH), and fluorine (–F), and $x$ is the number of surface functional groups [30,33,34]. Abundant functional groups clearly endow MXenes with multiple properties, including high surface areas, biocompatibility, hydrophilicity, low diffusion barriers, activated metallic hydroxide sites, superior electrical conductivity, and ease of tenability. On the other hand, MXene diversity has been greatly extended to more than 30 compositions through double or multiple combinations of transition

Received June 7, 2020; accepted July 25, 2020

E-mails: kanghuang@njtech.edu.cn (Huang K);
zhixu@ecust.edu.cn (Xu Z)

metals [31,35–37]. Multiple functional groups and diversity favor MXenes in energy-storage [33,38], sensor [39,40], optoelectronics [36], catalysis [41], environment-treatment [42,43], biomedicine [5], and supercapacitor applications [44]. Naturally, based on their laminar structures and abundant functionalities, MXenes have gradually become significantly attractive 2D membrane materials [45–52]. Their laminar structures endow 2D MXene membranes with special mass-transport channels, with water and other molecules moving rapidly in these limited domains. At the same time, the abundance of functional groups enables the separating ability of an MXene membrane to be readily adjusted by controlling the interlayer spaces [53], the affinity of the membrane for specific solvents [54], and the charge distribution [55]. While a preliminary review of the applications of normal MXene membranes has appeared in the literature [56], a systematic understanding of membrane performance, promotion strategies based on regulating the microstructures of laminar MXene membranes, and ways of expanding MXene applications are unfortunately lacking. This targeted mini-review not only provides a comprehensive overview of the assembly and separation mechanisms of MXene membranes, but also focuses on strategies proposed to further improve membrane performance and attempts made to expand MXene applications to date.

Recent major advances in 2D MXene-based membranes, in terms of applications and strategies, are summarized in Fig. 1. Relevant MXene-based membrane studies are summarized in Tables 1–3 based on ion-sieving, gas-molecule sieving, and small-molecule sieving, respectively. The corresponding sieving mechanisms are discussed in terms of the various separation processes. New horizons for MXene-based membranes are highlighted in this mini-review from four aspects, including MXene nanosheet cross-linking, constructing additional nanochannels, MXene hybrid membranes, and MXenes as 2D scaffolds.

## 2 MXene synthesis and assembly

### 2.1 MXene synthesis

MAX phases built by hexagonal layered $P6_3/mmc$-symmetric structures are composed of M–A and M–X bonds [40]. Accordion-like MXenes are successfully prepared by selectively etching weaker M–A bonds (purely metallic in nature) and retaining M–X bonds (covalent/metallic/ionic bonds) [31]. As shown in Fig. 2, the first reported 2D MXene material ($Ti_3C_2T_x$, which has attracted more than 70% of all MXene research attention to date) is synthesized by etching the Al layer in the $Ti_3AlC_2$ MAX phase [30]. In a typical synthesis procedure, the MAX powder is added to aqueous HF and stirred for a specific time. The reaction product is then washed several times

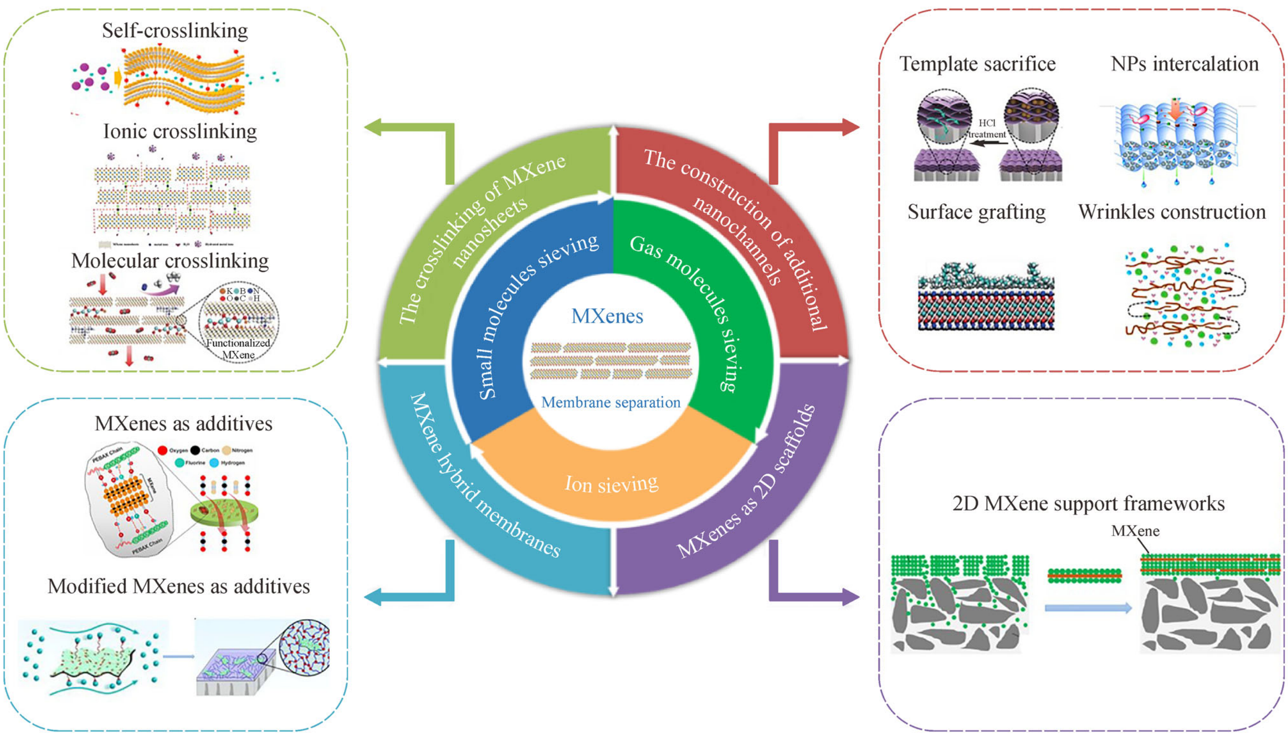


**Fig. 1** Scope of this mini-review. Based on various separation processes, this mini-review covers four main aspects for improving MXene-based membranes, including the crosslinking of MXene nanosheets. Reproduced with permission from refs. [46,49,54,57–62].

**Table 1** MXene-based membranes for ion sieving

| MXene sample | Methods | Support | Improved strategy | Applications | Separation performances (water flux, ion rejection) | Ref. |
|---|---|---|---|---|---|---|
| $Ti_3C_2T_x$ membrane | VF[a)] | PVDF[b)] | | Ion sieving (size and charge effect) | | [45] |
| $Ti_3C_2T_x$ membrane | VF[a)] | PAN[c)] | | Ion sieving (PV desalination) | 85.4 $L\cdot m^{-2}\cdot h^{-1}$, 99.5% (NaCl) | [63] |
| $Ti_3C_2T_x$ membrane | VF[a)] | | Surface grafting (PDDA[d)]) | Ion sieving (OEG[e)]) | | [55] |
| $Ti_3C_2T_x$ membrane | VF[a)] | Cellulose acetate | | Ion sieving (OEG[e)]) | | [64] |
| $Ti_3C_2T_x$/Kevlar hybrid membrane | VF[a)] | | Molecular crosslinking | Ion sieving (OEG[e)]) | | [65] |
| $Ti_3C_2T_x$ membrane | VF[a)] | Polypropylene | | Ion sieving | | [66] |
| $Ti_3C_2T_x$ membrane | VF[a)] | Polyamide | Self-crosslinking | Ion sieving | 0.0515 $L\cdot m^{-2}\cdot h^{-1}\cdot bar^{-1}$, 98% | [57] |
| $Ti_3C_2T_x$ membrane | VF[a)] | $\alpha$-$Al_2O_3$ tubular | Self-crosslinking | Ion sieving | 11.5 $L\cdot m^{-2}\cdot h^{-1}\cdot bar^{-1}$, 99.2% ($VO^{2+}$) | [53] |
| $Ti_3C_2T_x$/maleic acid membrane | VF[a)] | Nylon | Molecular crosslinking | Ion sieving | 22.8 $kg\cdot m^{-2}\cdot h^{-1}\cdot bar^{-1}$, > 99.7% (NaCl) | [67] |
| $Ti_3C_2T_x$ membrane | VF[a)] | PES[f)] | Ionic crosslinking ($Al^{3+}$) | Ion sieving | 2.8 $L\cdot m^{-2}\cdot h^{-1}\cdot bar^{-1}$, 96% (NaCl) | [68] |

a) VF: vacuum filtration; b) PVDF: polyvinylidene difluoride; c) PAN: polyacrylonitrile; d) PDDA: polydiallyl dimethyl ammonium; e) OEG: osmotic energy generation; f) PES: polyethersulfone.

**Table 2** MXene-based membranes for gas molecules sieving and PV

| MXene sample | Methods | Support | Improved strategy | Applications | Separation performances | Ref. |
|---|---|---|---|---|---|---|
| $Ti_3C_2T_x$ membrane | VF[a)] | | | Gas molecules sieving | $H_2$ permeability: 1201 GPU, $\alpha(H_2/CO_2) > 160$ | [47] |
| $Ti_3C_2T_x$ membrane (simulation) | VF[a)] | | | Gas molecules sieving | | [69] |
| $Ti_3C_2T_x$ membrane | VF[a)] | AAO[b)] | Self-crosslinking | Gas molecules sieving | $H_2$ permeability: 612.7 GPU, $\alpha(H_2/N_2)$: 41 | [70] |
| $Ti_3C_2T_x$ membrane (simulation) | VF[a)] | AAO[b)] | Self-crosslinking | Gas molecules sieving | | [71] |
| $Ti_3C_2T_x$ membrane | VF[a)] | AAO[b)] | Molecular crosslinking (PEI[c)]/borate) | Gas molecules sieving | $H_2$ permeability: 1584 GPU, $\alpha(H_2/CO_2)$: 27; $CO_2$ permeability: 350 GPU, $\alpha(CO_2/CH_4)$: 15.3 | [49] |
| $Ti_3C_2T_x$/pebax1657 hybrid membrane | Dc[d)] | PVDF[e)] | MXene as additives | Gas molecules sieving | $CO_2$ permeability: 1360 GPU, $\alpha(CO_2/N_2)$: 31 | [60] |
| $Ti_3C_2T_x$/pebax hybrid membrane | SC[f)] | PAN[g)] | MXene as additives | Gas molecules sieving | $CO_2$ permeability: 21.6 GPU, $\alpha(CO_2/N_2)$: 72.5 | [72] |
| $Ti_3C_2T_x$ membrane | VF[a)] | Nylon | | EtOH[h)] dehydration | Water flux: 263.4 $g\cdot m^{-2}\cdot h^{-1}$, separation factor: 135.2 | [73] |
| $Ti_3C_2T_x$/sodium alginate hybrid membrane | Dc[d)] | PAN[g)] | MXene as additives | EtOH[h)] dehydration | Water flux: 505 $g\cdot m^{-2}\cdot h^{-1}$, separation factor: 9946 | [74] |
| $Ti_2C_2T_x$ membrane | VF[a)] | PAN[g)] | Molecular crosslinking (HPEI[i)]) | IPA[j)] dehydration | Water flux: 1069±47 $g\cdot m^{-2}\cdot h^{-1}$, permeate side > 99 wt-% | [75] |
| $Ti_3C_2T_x$/chitosan hybrid membrane | SC[f)] | PAN[g)] | MXene as additives | Solvent dehydration | Water flux: 1.4–1.5 $kg\cdot m^{-2}\cdot h^{-1}$, separation factor: 1421, 4898, 906 (EtOH[h)], EAC[k)], DMC[l)]) | [76] |
| $Ti_2C_2T_x$ membrane | VF[a)] | PAN[g)] | Molecular crosslinking (PEI[c)], PDDA[m)], PAH[n)]) | IPA[j)] dehydration | Water flux: 1237 $g\cdot m^{-2}\cdot h^{-1}$, separation factor: 1932 | [77] |

a) VF: vacuum filtration; b) AAO: anodic aluminum oxide; c) PEI: polyethyleneimine; d) Dc: drop-casting; e) PVDF: polyvinylidene difluoride; f) SC: spin-coating; g) PAN: polyacrylonitrile; h) EtOH: ethanol; i) HPEI: hyperbranched polyethylenimine; j) IPA: isopropanol; k) EAC: ethyl acetate; l) DMC: dimethyl carbonate; m) PDDA: polydiallyl dimethyl ammonium; n) PAH: polyallylamine hydrochloride.

**Table 3** MXene-based membranes for small molecules sieving

| MXene sample | Method | Support | Improved strategy | Applications | Separation performances (flux, rejection) | Ref. |
|---|---|---|---|---|---|---|
| $Ti_3C_2T_x$/GO membranes | VF[a)] | Nylon/cellulose acetate | | SMS[b)] | 2.1, 0.3, 0.67, 0.23 $L \cdot m^{-2} \cdot h^{-1} \cdot bar^{-1}$ ($H_2O$), 68%, 99.5%, 93.5%, 100% (MR[c)], MB[d)], Rb[e)], BB[f)]) | [78] |
| $Ti_3C_2T_x$ membrane | VF[a)] | PVDF[g)] | Molecular crosslinking | SMS[b)] | 887 $L \cdot m^{-2} \cdot h^{-1} \cdot bar^{-1}$ ($H_2O$), > 99.4% (Oil) | [52] |
| $Ti_3C_2T_x$ membrane | VF[a)] | Commercial papers | | SMS[b)] | 450 $L \cdot m^{-2} \cdot h^{-1} \cdot bar^{-1}$ ($H_2O$), > 99% (Oil) | [51] |
| $Ti_3C_2T_x$ membrane | VF[a)] | PES[h)] | | SMS[b)] | 540 $L \cdot m^{-2} \cdot h^{-1} \cdot bar^{-1}$ ($H_2O$), 99.94% (Oil) | [48] |
| $Ti_3C_2$ membrane | VF[a)] | Glass fiber | | Li-S battery | | [79] |
| $Ti_3C_2T_x$ membrane | VF[a)] | Mixed cellulose ester | | SMS[b)] | 28.94±0.74 $L \cdot m^{-2} \cdot h^{-1} \cdot bar^{-1}$ ($H_2O$), 100±0.1% (MB[d)]) | [80] |
| $Ti_3C_2T_x$ membrane | VF[a)] | PES[h)] | | SMS[b)] | 115 $L \cdot m^{-2} \cdot h^{-1} \cdot bar^{-1}$ ($H_2O$), 92.3% (CR[i)]) | [81] |
| $Ti_3C_2T_x$ membrane | VF[a)] | Nylon | Wrinkles construction | SMS[b)] | 70, 64, 61 $L \cdot m^{-2} \cdot h^{-1} \cdot bar^{-1}$ ($H_2O$), 76.4%, 67.7%, 84.3% (AY14[j)], EY[k)], EB[l)]) | [58] |
| Ag@$Ti_3C_2T_x$ membrane | VF[a)] | PVDF[g)] | NPs intercalation | SMS[b)] | 387.05, 354.29, 345.81 $L \cdot m^{-2} \cdot h^{-1} \cdot bar^{-1}$ ($H_2O$), 79.93%, 92.32%, 100% (RB[m)], MG[n)], BSA[o)]) | [59] |
| $Ti_3C_2T_x$ membrane | VF[a)] | AAO[p)] | Template sacrifice method | SMS[b)] | > 1000 $L \cdot m^{-2} \cdot h^{-1} \cdot bar^{-1}$ ($H_2O$), > 90% (size large than 2.5 nm) | [46] |
| $TiO_2$-$Ti_3C_2T_x$ membrane | DC[q)] | Hollow fiber | 2D scaffolds | SMS[b)] | 90 $L \cdot m^{-2} \cdot h^{-1} \cdot bar^{-1}$ ($H_2O$), > 22000 Da (dextran) | [62] |
| $TiO_2$-$Ti_3C_2T_x$ membrane | DC[q)] | Hollow fiber | 2D scaffolds | SMS[b)] | 102 $L \cdot m^{-2} \cdot h^{-1} \cdot bar^{-1}$ ($H_2O$), 14854 Da (dextran) | [82] |
| $Ti_3C_2T_x$/PAN[r)] hybrid membrane | ES[s)] | | MXene as additives | SMS[b)] | Pressure drop: 42 Pa, 99.7% (PM2.5) | [83] |
| $Ti_3C_2T_x$/GO membrane | VF[a)] | Nylon | | SMS[b)] | 21.02, 48.32, 25.03, 10.76, 6.18 $L \cdot m^{-2} \cdot h^{-1} \cdot bar^{-1}$ ($H_2O$, CP[t)], MeOH[u)], EtOH[v)], IPA[w)]), > 90% | [23] |
| $Ti_3C_2T_x$ membrane | VF[a)] | Nylon | Surface grafting | SMS[b)] | 3337, 3018 $L \cdot m^{-2} \cdot h^{-1} \cdot bar^{-1}$ (ACN[x)], MeOH[u)]), > 92%, (MB[d)]) | [54] |
| $Ti_3C_2T_x$/(PEI[y)]/PDMS[z)]) hybrid membrane | Dc[a1)] | PAN[r)] | Modified MXene as additives | SMS[b)] | PEI[y)] membrane: 2.6, 0.3 $L \cdot m^{-2} \cdot h^{-1} \cdot bar^{-1}$ (IPA[w)], N/A[a1)]), 96%, 800 Da (PEG[b1)], 10 bar); PDMS[z)] membrane: 0.3, 1.5 $L \cdot m^{-2} \cdot h^{-1} \cdot bar^{-1}$ (IPA[w)], N/A[a1)]), 97%, 800 Da (PEG[b1)], 10 bar) | [61] |
| $Ti_3C_2T_x$/(PEI[y)]/PDMS[z)]) hybrid membrane | Dc[a1)] | PAN[r)] | MXene as additives | SMS[b)] | PEI[y)] membrane: 25.8, 19.1, 15.1, 6.4 $L \cdot m^{-2} \cdot h^{-1} \cdot bar^{-1}$ (IPA[w)], EAC[c1)], MEK[d1)], N/A[e1)]), 200 Da; PDMS[z)] membrane: 19.8, 14.9 $L \cdot m^{-2} \cdot h^{-1} \cdot bar^{-1}$ (TL[f1)], EAC[c1)]), 320 Da | [84] |
| $Ti_3C_2T_x$/P84[g1)] hybrid membrane | PI[h1)] | | MXene as additives | SMS[b)] | 268 $L \cdot m^{-2} \cdot h^{-1} \cdot bar^{-1}$ ($H_2O$), 408 Da (GV[i1)]) | [85] |
| RGO[j1)]/PDA[k1)]/MXene hybrid membrane | VF[a)] | Nylon | | SMS[b)] | > 200 $L \cdot m^{-2} \cdot h^{-1} \cdot bar^{-1}$ ($H_2O$), > 96% (MB[d)], MO[l1)], MR[c)], CR[i)], EB[l)]) | |

a) VF: vacuum filtration; b) SMS: small molecules sieving; c) MR: methyl red; d) MB: methylene blue; e) Rb: rose bengal; f) BB: brilliant blue; g) PVDF: polyvinylidene difluoride; h) PES: polyethersulfone; i) CR: congo red; j) AY14: acid yellow 14; k) EY: eosin Y; l) EB: evans blue; m) RB: rhodamine B; n) MG: methyl green; o) BSA: bovine serum albumin; p) AAO: anodic aluminum oxide; q) DC: dip-coating; r) PAN: polyacrylonitrile; s) ES: electro-spinning; t) CP: acetone; u) MeOH: methanol; v) EtOH: ethanol; w) IPA: isopropanol; x) ACN: acetonitrile; y) PEI: polyethyleneimine; z) PDMS: polydimethylsiloxane; a1) Dc: drop-casting; b1) PEG: polyethylene glycol; c1) EAC: ethyl acetate; d1) MEK: butanone; e1) N/A: *n*-heptane; f1) TL: toluene; g1) P84: polyimide; h1) PI: phase inversion; i1) GV: gentian violet; j1) RGO: reduced graphene oxide; k1) PDA: polydopamine; l1) MO: methyl orange.

with distilled water by centrifugation to achieve a pH of 4–6 [2,30,32]. The M–A bonds are destroyed by HF and the Al atoms are replaced by F, O, and OH atoms/groups. The relatively weak hydrogen and van der Waals bonds enable loosely packed MXenes to readily be delaminated by ultrasound and intercalated with large cations [40,42]. A suitable reaction temperature, HF concentration, etching time, and MAX-phase particle size are all vital for the production of high-quality MXenes in high yields [40]. A simplified freezing and thawing approach was recently effectively used to exfoliate multilayer MXenes in remarkably high yields [44].

To reduce the risk of hazardous HF, an *in-situ* HF formation strategy based on the reaction of LiF with HCl has been implemented, which is safer, easier, faster, and higher yielding [33]. Furthermore, researchers prefer to not to use F-containing compounds to avoid possible contamination. The selective electro-chemical etching method

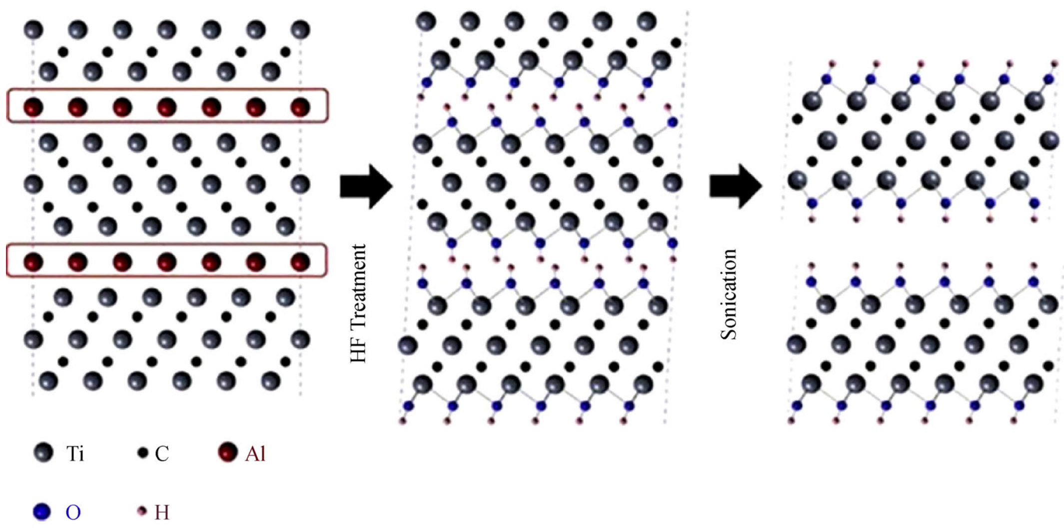


**Fig. 2** Schematic depicting the typical etching and sonication process for MXene ($Ti_3C_2T_x$) synthesis. Reproduced with permission from ref. [30]. Copyright 2011 Wiley-VCH GmbH, Weinheim.

recently developed for the synthesis of the $Ti_2CT_x$ MXene is hard to scale up, but is a meaningful fluoride-free synthesis route [86]. Another fluorine-free method, which uses molten $ZnCl_2$ salt to prepare new MAX phases, also represents an important advance that broadens experimental research on fluorine-free MXenes [87].

## 2.2 MXene nanosheet assembly

Surface-terminating functional groups (–O, –OH, and –F) endow MXenes with negative charge, which effectively hinders single-layered MXene nanosheets from overlapping and aggregating in solution for several months due to strong electrostatic repulsion [88,89]. Laminar MXene membranes are mainly prepared by facile vacuum filtration; once MXene nanosheets are stacked together, they become interlocked in a parallel fashion that leads to the assembly of the robust MXene membrane [90]. Possible mechanisms for the formation of 2D MXene membranes may be similar to those for GO-based membranes [91]. Compression generated by external force reduces the inter-layer spacing between MXene nanosheets; consequently, MXene nanosheets are oriented perpendicular to the direction of extraction and form highly ordered parallel layers. This process is also affected by interactions between functional groups. On one hand, electrostatic repulsion between adjacent MXene nanosheets prevents random assembly, while on the other hand, the formation of hydrogen bonds between functional groups reduces the tendency of MXene nanosheets to dissociate. Membrane thickness depends on material load of MXene nanosheets. When additives, such as small molecules and nanoparticles (NPs), are introduced in the aforementioned assembly process, they interact with the MXene nanosheets to facilitate the formation of the required composite structure [46,75].

In addition to above-mentioned methods, MXene hybrid membranes have also been assembled by thoroughly blending MXenes with polymers; the chemical bonds formed between the oxygen-containing functional groups on an MXene and a polymer significantly reduce polymer-chain mobility and create well-formed galleries for molecular transport [60]. To date, MXene hybrid membranes have usually been prepared by drop-casting [61], spin-coating [72], phase-inversion [85], and electrospinning [83] methods.

## 2.3 Lamella properties of MXene

The narrow interlayer spacings formed by regular MXene nanosheets are highly versatile and facilitate the transport of small molecules while impeding molecules that are larger than the layer spacing [56]. This size-effect phenomenon is mainly responsible for the abilities of MXene lamellas to separate. Gogotsi et al., the discoverers of MXene [45], were the first to investigate the molecular sieving abilities of MXene ($Ti_3C_2T_x$) membranes. The confined transport channels in MXene membranes effectively exclude molecules larger than the interlayer distance (~6.4 Å); for example, $MB^+$ (Methylene Blue) showed almost no permeation (only $7 \times 10^{-4}$ $mol \cdot h^{-1} \cdot m^{-2}$). Similarly, Ding et al. [46] prepared an anodic aluminum-oxide-supported MXene membrane that exhibited excellent water permeance (more than 1000 $L \cdot m^{-2} \cdot h^{-1} \cdot bar^{-1}$) and excellent rejection rates (over 90 %) for molecules larger than 2.5 nm (Fig. 3(a)). Zhang et al. [80] also recently developed an MXene membrane for dye rejection that exhibited outstanding performance (dye water flux: 44.97 ± 2.19 $L \cdot m^{-2} \cdot h^{-1} \cdot bar^{-1}$; dye removal: 100% ± 0.1%, MB) at a feed concentration of 75 $mg \cdot L^{-1}$. They found that dye removal was affected by the adsorption capacity of the MXene membrane at the start of the experiment. In addition to dye adsorption, the size effect was observed to play a leading role when dye molecules occupy all adsorption sites, with slightly lower rejection rates observed. The decrease in water flux was attributed to the rejected dye molecules accumulating around the MXene edges and resisting water transport. The size effect in MXene membranes has also been demonstrated in pervaporation (PV) desalination processes. Liu et al. [63] found that MXene membranes with interlayer distances of 0.35 nm selectively transported water molecules with kinetic diameters of 0.29 nm and resisted other larger ions; higher water fluxes were achieved by MXene membranes with smaller MXene nanosheets due to their relatively loose stacking structures. In addition, MXene membranes were also used to suppress lithium polysulfide (LiPS) shuttling in a Li-S battery based on the size effect of MXene lamellas, which act as an additional conductive network as well as a LiPSs reservoir [79]. The discharge capacity of the Li-S battery was enhanced by a factor of 15 when glass fibers were covered with few-layer MXene nanosheets by vacuum filtration (Fig. 3(b)).

In addition to the size effect, the surface charge of the MXene nanosheet also greatly affects the separation performance of the membrane. For example, Ren et al. [45] found that MXene membranes are significantly more selective toward differently charged cations compared to GO (Fig. 4(a)). Singly charged ions (such as $K^+$ and $Na^+$) are able to pass through the channels in an unimpeded manner. More importantly, they attract to both faces of the MXene nanosheets to form electric double layers, thereby effectively increasing the interlayer distance and facilitating water transport (Fig. 4(b)) [45]. However, multiply charged cations ($Mg^{2+}$, $Ca^{2+}$, and $Al^{3+}$) that have radii slightly smaller than the interlayer distance only slowly migrate into the channels. Meanwhile, the shrinkage of adjacent MXene nanosheets further prevents any increase in permeation due to electrostatic attraction between these cations and the negatively charged MXene surfaces. Therefore, $Na^+$ (1.53 $mol \cdot h^{-1} \cdot m^{-2}$) was found to permeate 7-times faster than $Ca^{2+}$, and 25-times faster than $Al^{3+}$.

Thirdly, the specific affinities of adjacent MXene nanosheets for gas molecules also facilitate molecular transport or buffer their movement by adsorption. For example, Ding et al. [47] first demonstrated the potential abilities of 2D MXene materials to sieve gas molecules using the size effect and the affinities of MXenes for $CO_2$. Self-supporting MXene membranes (Fig. 5(a)) with a *d*-spacing of 0.35 nm were prepared to sieve gaseous He, $H_2$, $CO_2$, and $O_2$, among others; they exhibited excellent permeabilities and selectivities for hydrogen ($H_2$ permeance = 1201 GPU; $H_2/CO_2$ selectivity > 160, Fig. 5(b)). Molecular dynamics (MD) simulations [69] revealed that the *D* (diffusion coefficient) values of He and $H_2$ in tightly stacking MXene membranes ($d < 6$Å) were one-to-three orders of magnitude higher than those of molecules with large kinetics diameters (e.g., $CO_2$, $N_2$ and $CH_4$), consequently, clear cut-off behavior between $H_2$ and larger gas molecules was observed. In particular, $CO_2$ molecules moved more slowly (lower diffusivity) due to the higher quadrupole and polarizability of $CO_2$. A similar phenomenon was also observed by Shen et al. [49]; an ultrathin (20-nm-thick) MXene membrane exhibited excellent $H_2$ separation performance ($H_2$ permeance = 1584 GPU; $H_2/CO_2$ selectivity > 27) that exceeded the 2008 Robeson upper-bound for polymeric

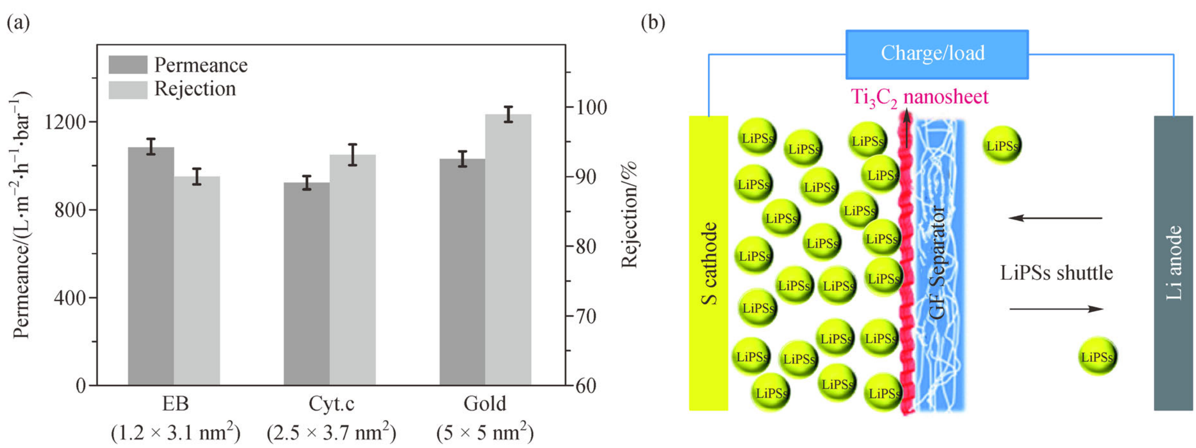


**Fig. 3** (a) Separation performance of MXene membranes for molecules with various sizes. Reproduced with permission from ref. [46]. Copyright 2017 Wiley-VCH GmbH, Weinheim; (b) schematic of LiPS shuttling in a Li-S battery with few-layered MXene nanosheets. Reproduced with permission from ref. [79]. Copyright 2016 Royal Society of Chemistry.

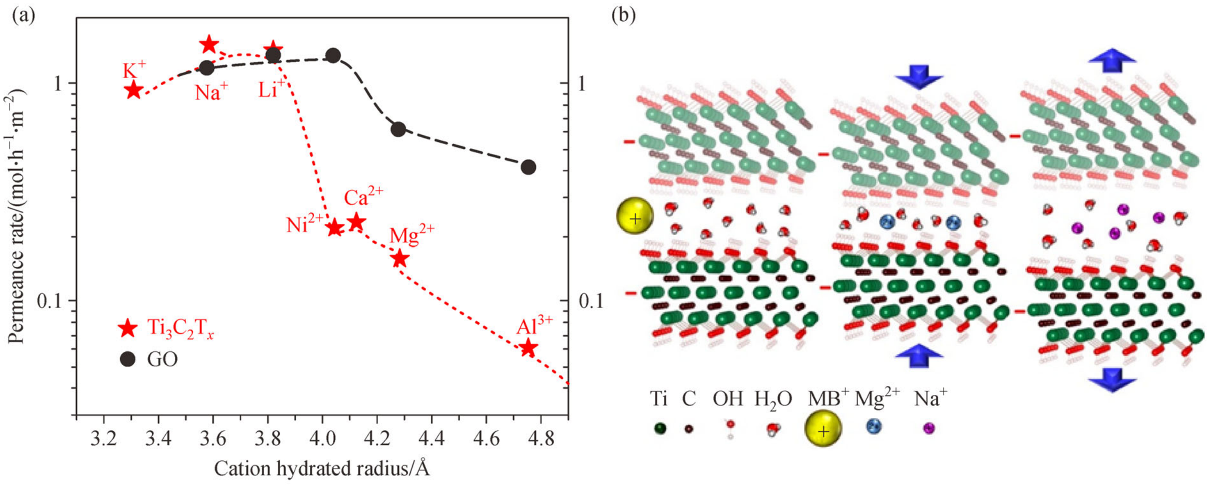


**Fig. 4** (a) Permeation rates of differently charge cations through GO and MXene ($Ti_3C_2T_x$) membranes; (b) permeation behavior of various cations through an MXene membrane. Reproduced with permission from ref. [45]. Copyright 2015 American Chemical Society.

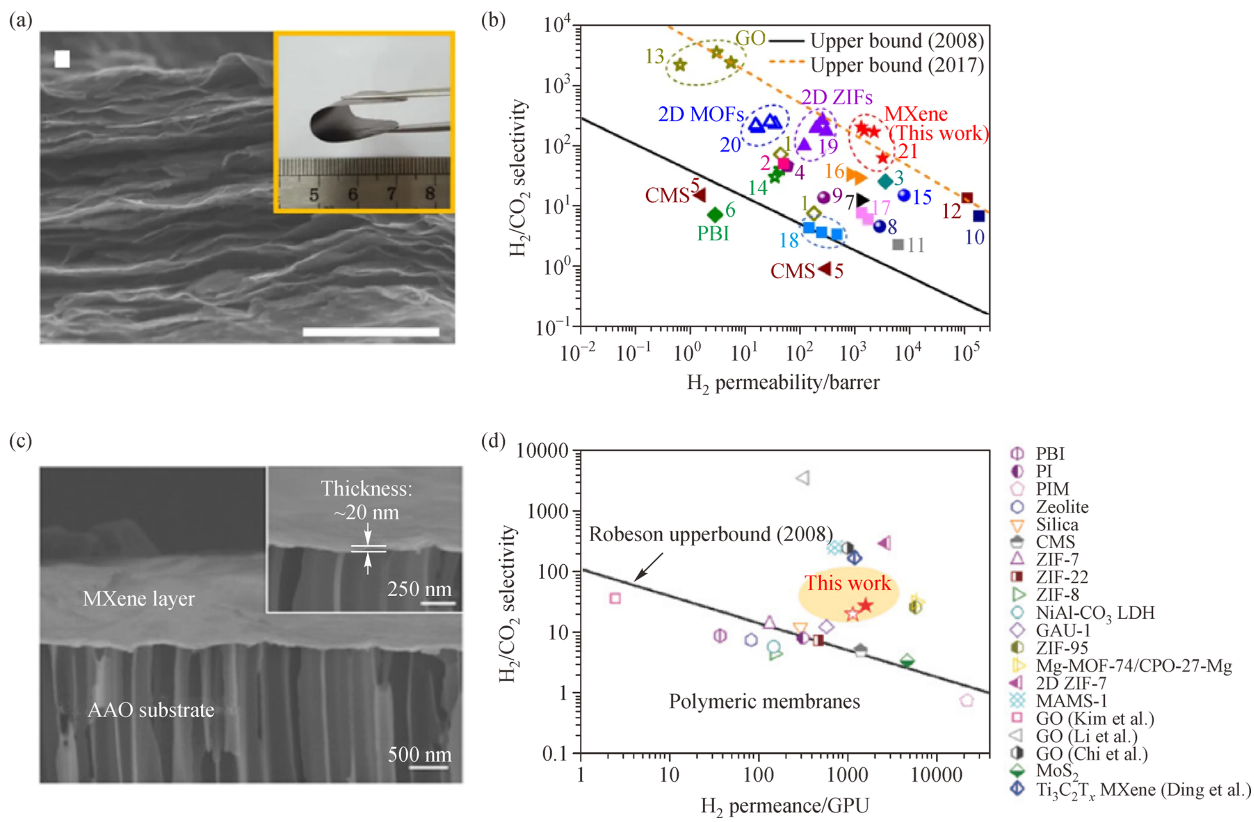


**Fig. 5** (a) Scanning electronic microscopy (SEM) image of a self-supporting MXene membrane; (b) comparing the $H_2/CO_2$ separation performance of a self-supporting MXene membrane and state-of-the-art gas-separation membranes. Reproduced with permission from ref. [47]. Copyright 2018 Springer-Verlag GmbH Germany; (c) cross-sectional SEM image of an ultrathin MXene membrane; (d) comparing the $H_2/CO_2$ separation performance of the ultrathin MXene membrane and state-of-the-art gas separation membranes. Reproduced with permission from ref. [49]. Copyright 2018 Wiley-VCH GmbH, Weinheim.

membranes (Figs. 5(c) and 5(d)).

With the exceptions of the above properties, the hydrophilicity and oleophobicity performance of MXene nanosheets can also be used to sieve small molecules, such as oil droplets. For instance, Saththasivam et al. [51] reported a pioneering study on the oil/water separation performance of a selective MXene ($Ti_3C_2T_x$) layer (Fig. 6(a)). Due to its superoleophobicity (contact angle: 137°) and suitable channel size, the membrane showed a sieving efficiency of 99% for an oil/water emulsion as well as an ultrahigh water flux of 450 $L \cdot m^{-2} \cdot h^{-1} \cdot bar^{-1}$. Li et al. [48] also prepared an ultra-thin MXene membrane with excellent oil/water emulsion-separation performance (Fig. 6(b)). Moreover, these MXene membranes showed higher oil rejection for salt-containing oily wastewater due to ion intercalation that reduced the interlayer spacing.

## 3 Designing MXene-based membranes

Compared with traditional polymer and ceramic membranes, 2D MXene membranes have numerous distinguished properties, such as hydrophilism, flexibility, and superior mechanical strength [88,92]. The randomly distributed nanowrinkles and interlayer spacings derived from abundant terminating functional groups (oxygen (=O), hydroxyl (–OH), and fluorine (–F)) form interconnected nanochannels for gas molecules, ions, and other small molecules [47,58,63,70,71,79]. To date, MXene membranes have shown great potential in molecular-separation applications, such as gas separation [47,49], desalination [45,63], and wastewater treatment [80,81]. However, shortcomings, such as the uncompetitive water fluxes of MXene membranes, as well as poor stability and mechanical strength due to membrane swelling and imperfect stacking, still limit their applications in practical separation processes. A series of strategies have been proposed by researchers to deal with these challenges and significantly enhance the permeabilities, stabilities, and strengths of 2D MXene membranes. MXenes also can be used as additives to form MXene hybrid membranes. The introduction of MXene nanosheets improves molecular transport in a polymer membrane, while acting as versatile platforms for specific polymer membrane functionalities. In addition, MXenes can be used as 2D scaffolds to assist and improve membrane preparation processes.

### 3.1 Cross-linking MXene nanosheets

While the water-swelling behavior of MXene lamellas favors high permeation fluxes, the correspondingly larger *d*-spacing partially weakens sieving performance and decreases the stability of the MXene membrane [45]. The degree of water swelling needs to be controlled to provide an excellent balance between permeability and selectivity. Fortunately, the abundant oxygen-containing functional groups on MXene nanosheets endow them with sufficient flexibility in this regard due to their high reactivities and abilities to be modified. To date, several chemical cross-linking techniques, such as self-cross-linking [53,57], molecular crosslinking [67,75], and ionic crosslinking [68], have been used to adjust the water-swelling behavior of MXene stacks in order to improve the quality and separation performance of MXene membranes. Lu et al. [57] developed a self-crosslinked MXene membrane with outstanding ion-rejection performance and stability. Facile thermal treatment led to dehydration reactions involving hydroxyl functional groups on adjacent MXene nanosheets, which resulted in interlocked structures (Fig. 7(a)). Due to the reduced *d*-spacing, the

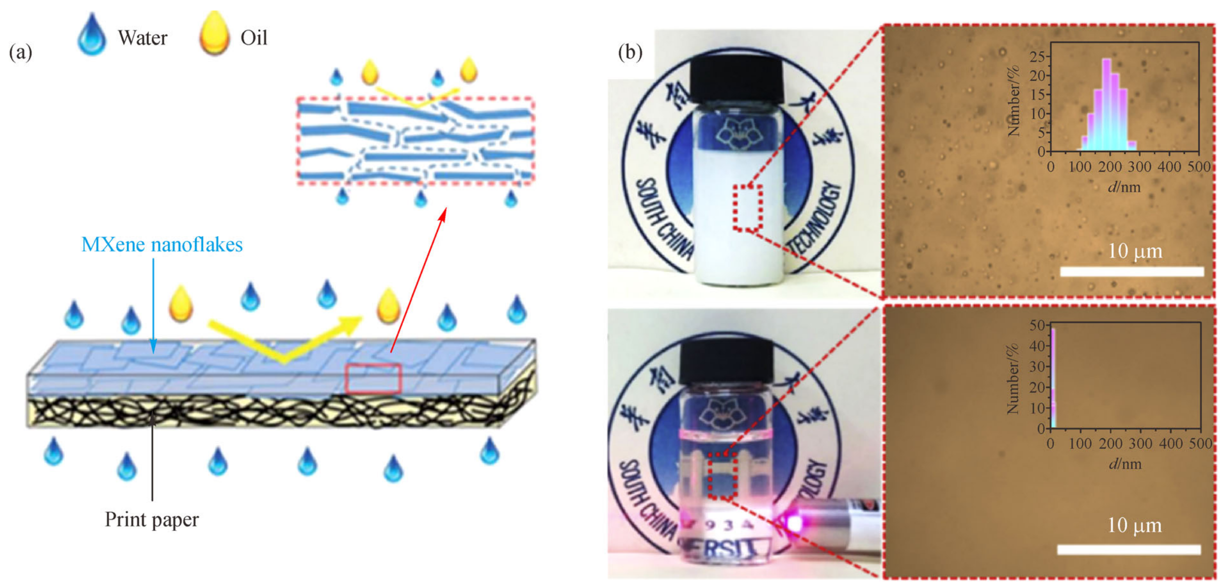


**Fig. 6** (a) Schematic illustration of an MXene membrane for oil droplet sieving. Reproduced with permission from ref. [51]. Copyright 2016 Royal Society of Chemistry; (b) photographic images of a toluene/water emulsion and the permeate after separation by an MXene membrane. Reproduced with permission from ref. [48]. Copyright 2019 Elsevier.

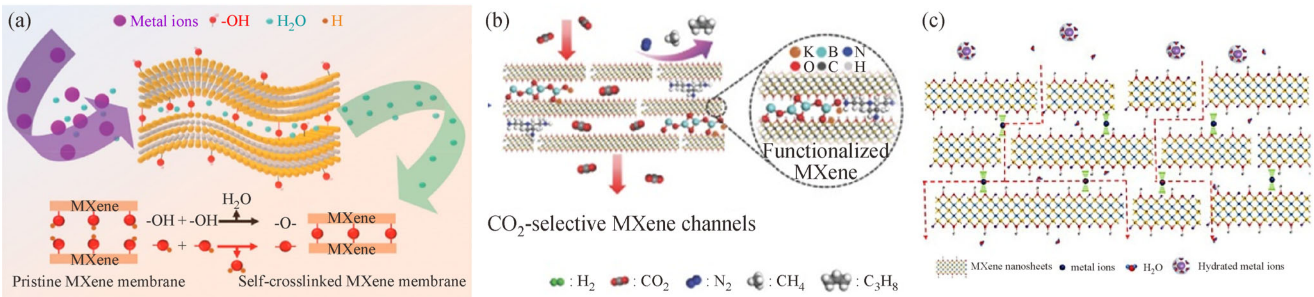


**Fig. 7** Schematics of cross-linked MXene ($Ti_3C_2T_x$) membranes formed by (a) self-crosslinking. Reproduced with permission from ref. [57]. Copyright 2019 American Chemical Society; (b) molecular crosslinking. Reproduced with permission from ref. [49]. Copyright 2018 Wiley-VCH GmbH, Weinheim; (c) ionic crosslinking.

ion-exclusion performance of the self-crosslinked MXene membrane was enhanced by a factor of at least 30 compared to that of the pristine MXene membrane. At the same time, the self-crosslinked MXene membrane exhibited excellent structural stability during ion separation. This self-crosslinking strategy is a facile and efficient method for improving the anti-swelling properties of many 2D materials with tunable functional groups.

On the other hand, the molecular crosslinking strategy not only forms interlocked structures that enhance structural stability, but it can also be used to introduce additional properties into MXene membranes that improve separation flexibility [55,67]. Liu et al. [75] intercalated positively charged hyperbranched polyethylenimine between negatively charged MXene nanosheets to dehydrate isopropanol by pervaporation. Highly ordered 2D stacked nanochannels were assembled through electrostatic interactions. On account of water sorption and size-sieving effects, these membranes showed a high water content ($>99\%$) in the permeate and similar high fluxes ($1069 \pm 47$ $g\cdot m^{-2}\cdot h^{-1}$). Moreover, crosslinking $CO_2$-philic molecules was shown to regulate the gas-sieving performance of an MXene membrane. Shen et al. [49] reported a 2D MXene membrane intercalated with $CO_2$-philic molecules and with tunable transport nanochannels for $CO_2$ capture, which highlighted the versatility and flexibility of the molecular crosslinking strategy (Fig. 7(b)). Pristine MXene membranes with large *d*-spacings were unable to discriminate between $CO_2$ (0.33 nm), $CH_4$ (0.38 nm), and $N_2$ (0.36 nm). Crosslinking with $CO_2$-philic molecules (such as borate and polyethylenimine) resulted in the reversible adsorption and release of $CO_2$ molecules in the MXene nanochannels, which facilitated their transport and enhanced selectivity for $CO_2$ over other molecules.

The abundant functional groups on the surfaces of MXene nanosheets can also form coordination bonds to metal ions (Fig. 7(c)), which can potentially be used to enhance the anti-swelling properties of MXene membranes through ionic crosslinking strategies [68]. Recently, Ding et al. [68] reported an $Al^{3+}$-intercalated MXene membrane with excellent anti-swelling properties. $Al^{3+}$ was intercalated into the pristine MXene membrane through concentration diffusion and adjacent MXene nanosheets locked by the formation of Al–O bonds. The swelling of the MXene membrane was clearly inhibited through strong interactions between the oxygen functional groups and $Al^{3+}$. The permeation rates of ions (e.g., $K^+$, $Na^+$, $Li^+$, $Ca^{2+}$, and $Mg^{2+}$) through the $Al^{3+}$-intercalated MXene membrane were two orders of magnitude lower than those of the pristine membrane, while also exhibiting outstanding anti-swelling properties in long-term stability testing in water for up to 400 h. The aforementioned three crosslinking strategies provide guidance for the development of high-quality nanosheet-based membranes.

### 3.2 Constructing additional nanochannels

MXene membranes have shown great promise in terms of separation performance, however MXene membrane permeation still falls short of the requirements of a number of applications. Their channels are less fluidic (narrow interlayer spaces and few randomly distributed nanoscale wrinkles) and their slow diffusion rates greatly affect the ability to improve permeation performance. Constructing additional nanochannels has been an effective strategy for significantly improving permeability while retaining high rejection rates [46,58,59,93]. Recently, Xing et al. [58] prepared reinforced crumpled MXene lamellar membranes by a facile freeze-drying method (Fig. 8(a)); these membranes showed ultrafast water and organic solvent permeation due to the higher number of transport nanochannels provided by the wrinkles. In addition, the presence of interlayer NPs creates additional nanochannels or interlayer voids, facilitating water movement through shorter transport pathways. Pandey et al. [59] prepared an intercalated Ag@MXene membrane by the *in-situ* reduction of silver nitrate to Ag NPs (Fig. 8(b)). The water flux of the Ag@MXene membrane (21%) was more than four-times that of the pristine membrane for the rejection of rhodamine B (RhB), methyl green (MG), and bovine serum albumin (BSA). It is worth noting that the Ag NPs in

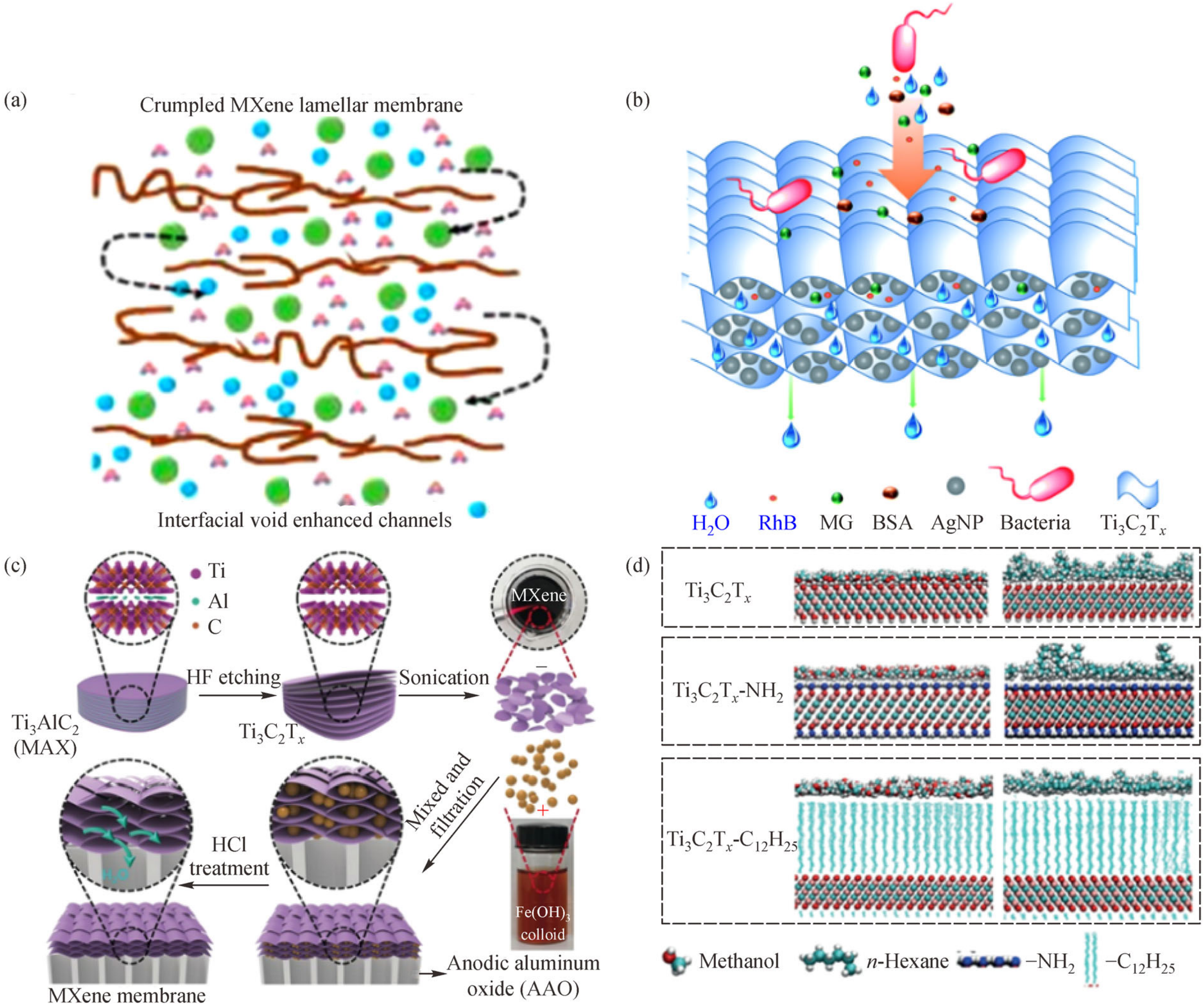


**Fig. 8** (a) Schematic of a crumpled MXene lamellar membrane. Reproduced with permission from ref. [58]. Copyright 2020 American Chemical Society; (b) schematic of an ultrahigh-flux and fouling-resistant membrane created by *in-situ* formed Ag NPs. Reproduced with permission from ref. [59]. Copyright 2018 Royal Society of Chemistry; (c) schematic of the preparation of a porous MXene membrane by the template-sacrifice method. Reproduced with permission from ref. [46]. Copyright 2017 Wiley-VCH GmbH, Weinheim; (d) schematic of molecular configurations within nanochannels (MD simulations). Reproduced with permission from ref. [54]. Copyright 2019 Wiley-VCH GmbH, Weinheim.

the MXene membrane concurrently deactivate pathogens to ensure penetration of high-quality water while prolonging the lifespan of the MXene membrane.

Transport resistance can be lowered by etching the NPs in the MXene membranes. Prior to the development of the freeze-drying and crumpling, and Ag NP assistance methods, Ding et al. [46] reported pioneering nanochanneled MXene membranes fabricated using $Fe(OH)_3$ NPs as sacrificial templates (Fig. 8(c)). The additional nanochannels and short transport pathways created by facile etching with HCl endowed these MXene membranes with ultrahigh water fluxes (5–10 times higher than those of the pristine MXene membrane) without sacrificing the rejection rate. Moreover, functional groups with affinities for specific molecules can be used to construct additional nanochannels between adjacent MXene nanosheets. Wu et al. [54] prepared MXene membranes by chemically grafting hydrophobic ($–C_6H_5$, $–C_{12}H_{25}$) and hydrophilic ($–NH_2$) groups (Fig. 8(d)). The MXene membranes with hydrophilic nanochannels exhibited ultra-high transmittances ($>3000\ L \cdot m^{-2} \cdot h^{-1} \cdot bar^{-1}$) for polar molecules, which were more than three-times higher than those for membranes with hydrophobic nanochannels, which is ascribable to polar molecules forming orderly aligned aggregates along the hydrophilic nanochannels, whereas they are arranged in a disorderly fashion in hydrophobic nanochannels.

### 3.3 MXene hybrid membranes

When MXenes are used as additives to form MXene hybrid membranes, the abundant functional groups on the

MXene surfaces chemically bond to the polymer chains to reduce the formation of interfacial defects. Meanwhile, small numbers of MXene nanosheets can assemble into several-layered MXene stacks with linear diffusion highways and interlayer spacings for molecular sieving. The strategy of introducing MXenes into polymer membranes has been shown to be effective for improving separation performance [60,61,72,74,76,85]. Xu et al. [76] fabricated an MXene/chitosan hybrid membrane for pervaporation dehydration by incorporating MXene nanosheets into chitosan. The added MXene nanosheets improved the selectivity for $H_2O$ diffusion over ethanol/ethyl acetate/dimethyl carbonate, leading to a remarkable enhancement in membrane performance (Fig. 9(a)). The MXene/chitosan hybrid membrane exhibited fluxes of 1.4–1.5 $kg \cdot m^{-2} \cdot h^{-1}$ and separation factors of 1421, 4898, and 906 for the dehydration of ethanol, ethyl acetate, and dimethyl carbonate at 50 °C. In addition, the introduction of MXene nanosheets into hybrid membranes also effectively enhanced their gas separation abilities. Shamsabadi et al. [60] prepared MXene hybrid membranes for $CO_2$ capture by embedding MXene ($Ti_3C_2T_x$) nanosheets in pebax 1657 (Fig. 9(b)). Due to the presence of high-speed selective $Ti_3C_2T_x$ nanochannels, the membrane enabled fast and selective $CO_2$ transport, which exceeded Robeson's upper bound. The same transport properties were observed for MXene hybrid membranes based on pebax 2533 and polyurethane, highlighting the universality of this strategy [60].

Moreover, MXene nanosheets can also be used as bridges for the introduction of other specific functionalities into polymer membranes. Hao et al. [61] prepared MXene hybrid membranes by adding multi-functional MXene nanosheets for specific solvent transport (Fig. 9(c)). Hybrid membranes containing MXene nanosheets modified by various functional groups showed very different solvent-transport behavior. Membranes containing $-NH_2$ and –COOR groups facilitated the transport of polar molecules,

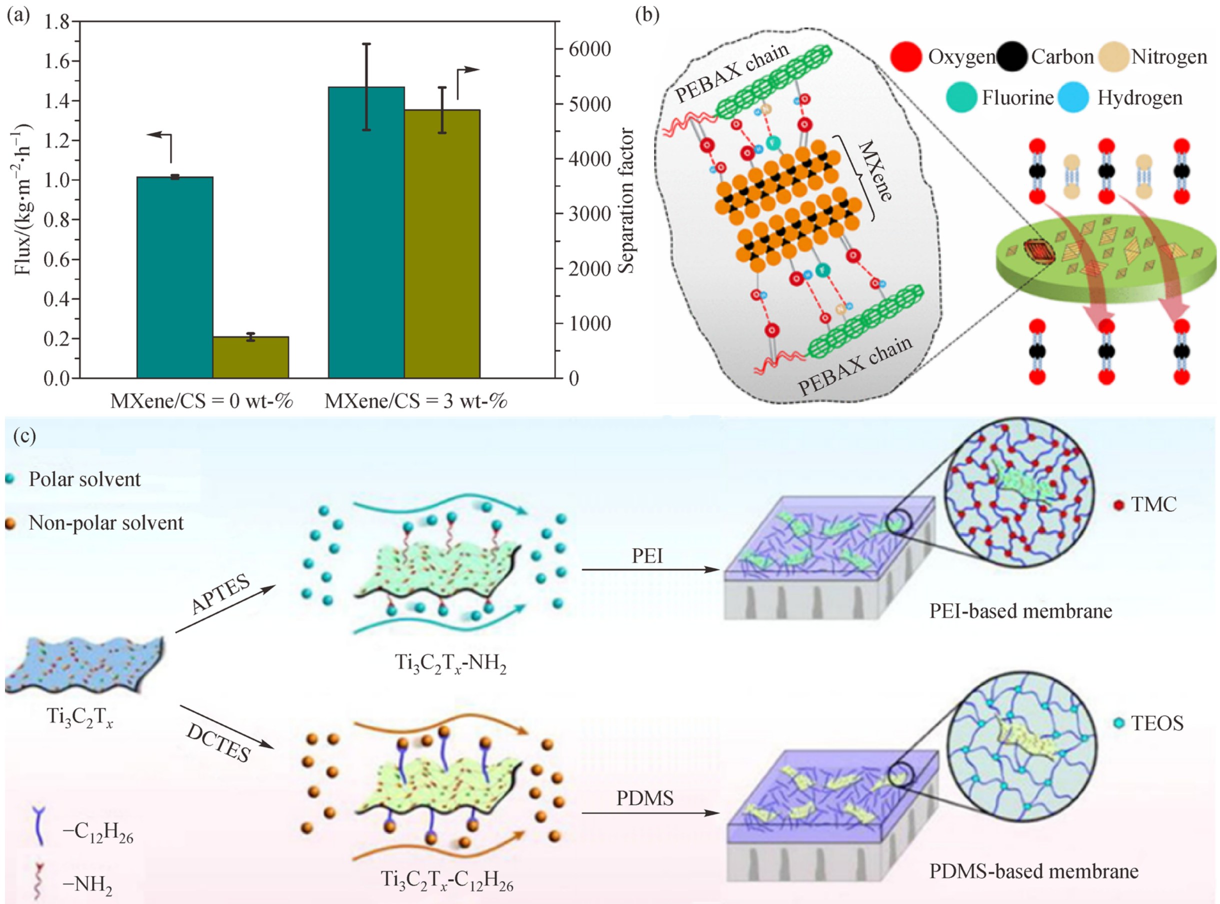


**Fig. 9** (a) Performance of 3 wt-% MXene/chitosan hybrid membrane for ethyl acetate dehydration. Reproduced with permission from ref. [76]. Copyright 2018 Elsevier; (b) schematic showing the hydrogen bonds between MXene ($Ti_3C_2T_x$) nanosheets and pebax chains. Reproduced with permission from ref. [60]. Copyright 2020 American Chemical Society; (c) schematic depicting MXene modification and the microstructures of MXene hybrid membranes based on various functional groups. Reproduced with permission from ref. [61]. Copyright 2017 Elsevier.

such as isopropanol, due to their affinities for polar molecules, while blocking non-polar solvent molecules. On the other hand, membranes with $–C_6H_6$ and $–C_{12}H_{26}$ groups exhibited the opposite behavior. The addition of MXene nanosheets effectively transfers the task-specific functionalities of the MXene to the hybrid membrane; this facile strategy provides guidance for the construction of task-specific membranes.

### 3.4 MXenes as 2D scaffolds

While the abundant functional groups of MXene nanosheets have been widely used to regulate membrane microstructures, the robust 2D assemblies of the MXene nanosheets themselves can be used as 2D support frameworks that facilitate the formation of inorganic membranes. For instance, the sol-gel method is commonly used to prepare inorganic mesoporous membranes [94,95]; however, the sols often suffer from serious penetration issues, a consequence of the larger support pores, which results in the formation of defects. A toughened network-structured gel that effectively reduces gel penetration was formed by introducing 2D nanosheets into a $TiO_2$ sol [96,97]. In this respect, Xu et al. successfully used the lamellar structures of MXenes to assist the sol-coating process [62]. As shown in Fig. 10, a $TiO_2$@MXene sol was prepared by rapidly mixing an MXene dispersion with a $TiO_2$ sol. The 3D support framework was formed by assembling the 2D MXene nanosheets and the $TiO_2$ NPs therein. The tendency to penetrate into the membrane support of the $TiO_2$@MXene sol was prevented by the "floor tile" effect of the MXene nanosheets. The designed mesoporous membrane supported by a 2D MXene framework exhibited outstanding separation performance, with a water flux of more than 90 $L \cdot m^{-2} \cdot h^{-1} \cdot bar^{-1}$ and a cut-off molecular weight of 22000 Da.

The introduced 2D MXene scaffolds also improve membrane separation performance. Sun et al. [82] investigated the roles of MXene nanosheets in MXene-$TiO_2$ mesoporous membranes. The addition of MXene nanosheets not only inhibited sol penetration during membrane preparation, but also provided longitudinal and lateral transport pathways for dextran between MXene nanosheets and $TiO_2$ NPs. The optimal mesoporous membranes showed excellent separation performance, with a water flux of more than 102 $L \cdot m^{-2} \cdot h^{-1} \cdot bar^{-1}$ and a cut-off molecular weight of 14854 Da.

## 4 Conclusions and outlook

MXenes have emerged as candidate materials with tremendous potential for membrane separation applications. In this timely mini-review, we systematically summarize the synthesis, separation mechanisms, and design strategies for MXene membranes. MXene separation mechanisms involved in gas molecule sieving, ion sieving, and small molecule sieving, as well as the latest strategies for enhancing separation performance (such as crosslinking and the construction of additional nanochannels) are especially emphasized. Recent progress in MXene-based membranes, where MXenes not only act as multifunctional additives but also as flexible 2D scaffolds, is also discussed. Although MXene membranes have shown excellent separation performance, their use in other membrane-separation applications, such as electrodialysis, forward osmosis, and as bipolar membranes, remains insufficiently developed and needs to be investi-

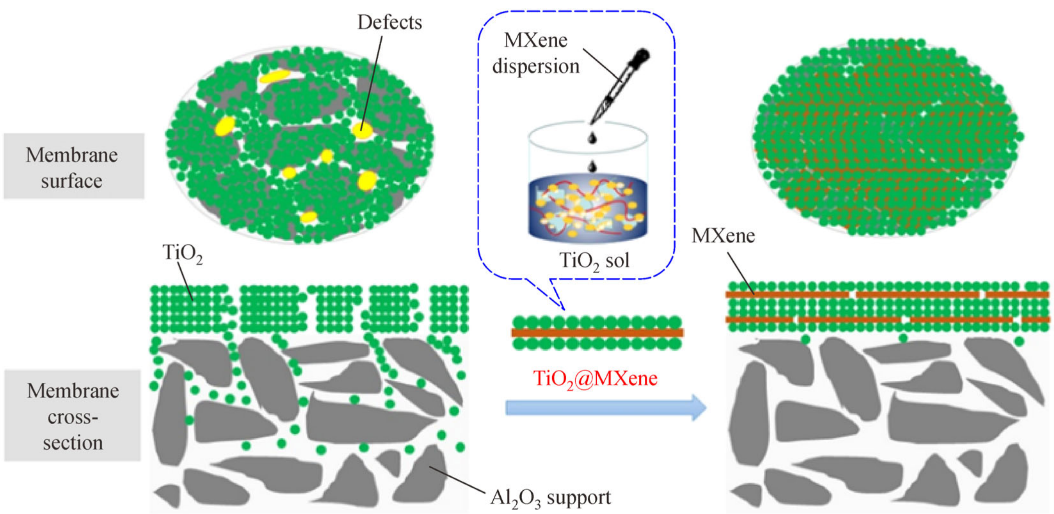


**Fig. 10** Schematic of the preparation process for a mesoporous $TiO_2$-MXene membrane. Reproduced with permission from ref. [62]. Copyright 2018 Elsevier.

gated for a variety of purposes by combing the properties and functions of MXene materials.

The abundant functional groups on the surfaces of MXenes are still the main sources of creative inspiration for solving the limitations encountered by membranes, such MXene oxidation, the lack of control over the interlayer space, membrane instability, and general unsatisfactory performance. Hydrogen annealing has been proven to be effective for suppressing MXene oxidation by partially sintering flakes at high temperatures, but the changes in the surface functional groups may disadvantage membrane preparation and modification [98]. Edge capping has been suggested as a method for selectively functionalizing the edges of MXene sheets in a different manner to their surfaces using polyanionic salts [99], which provides a reference for mitigating oxidation by surface modification. Modifying MXenes by grafting functional groups ($–C_6H_5$, $–C_{12}H_{25}$, and $–NH_2$, etc.) and crosslinking with molecules (PEI, PVA, borate, amine, pebax, maleic acid, and PDDA, etc.) has proven to be effective for enhancing MXene membrane stability and separation performance, but more attention needs to be paid to its oxidation-retarding effects. In addition, based on the flexibility provided by functional-group modification, more MXene-film applications, such as in analysis, detection, and drug-delivery systems, can be explored.

At the raw material stage, efficient etching methods are required to improve yields and, consequently, reduce costs and promote MXene membrane applications. In addition to traditional HF etching, two significant methods (water-free etching in a polar organic solvent and the freezing and thawing approach) have been developed to date. Moreover, while MXenes form a large family of materials, more than 70% of current MXene research is based on the first-discovered MXene; i.e., $Ti_3C_2T_x$. The majority of MXenes are underexplored and need to be developed for various applications, such as photoelectric devices [100], energy storage [33], and photocatalysis [101].

MXene applications also go far beyond those mentioned above, and to demonstrate their versatility we highlight the special applications of MXenes as 2D scaffolds. Moreover, further special uses of MXenes can be anticipated, such as in photo-thermal therapy [102], shape memory materials [103], and textile triboelectric nanogenerators [104], among others.

In a word, recent work on MXene membranes has revealed that they are advanced representatives of next-generation multifunctional membranes for task-specific sieving applications. Additional applications and improved MXene membrane strategies need to be explored in order to realize a bright future for this cutting-edge molecular separation field.

**Acknowledgements** We gratefully acknowledge the financial support from the National Natural Science Foundation of China (Grant Nos. 21908054 and 21908098).

## References

1. Novoselov K S, Geim A K, Morozov S V, Jiang D, Zhang Y, Dubonos S V, Grigorieva I V, Firsov A A. Electric field effect in atomically thin carbon films. Science, 2014, 306(5696): 666–669
2. Zhu J, Ha E, Zhao G L, Zhou Y, Huang D S, Yue G Z, Hu L S, Sun N, Wang Y, Lee L Y S, et al. Recent advance in MXenes: a promising 2D material for catalysis, sensor and chemical adsorption. Coordination Chemistry Reviews, 2017, 352: 306–327
3. Zhan X X, Si C, Zhou J, Sun Z M. MXene and MXene-based composites: synthesis, properties and environment-related applications. Nanoscale Horizons, 2020, 5(2): 235–258
4. Tang Q, Zhou Z. Graphene-analogous low-dimensional materials. Progress in Materials Science, 2013, 58(8): 1244–1315
5. Huang K, Li Z J, Lin J, Han G, Huang P. Two-dimensional transition metal carbides and nitrides (MXenes) for biomedical applications. Chemical Society Reviews, 2018, 47(14): 5109–5124
6. Cheng L, Guan K C, Liu G P, Jin W Q. Cysteamine-crosslinked graphene oxide membrane with enhanced hydrogen separation property. Journal of Membrane Science, 2020, 595: 117568
7. Cheng Y D, Wang X R, Jia C K, Wang Y X, Zhai L Z, Wang Q, Zhao D. Ultrathin mixed matrix membranes containing two-dimensional metalorganic framework nanosheets for efficient $CO_2$/$CH_4$ separation. Journal of Membrane Science, 2017, 539: 213–223
8. Lu P, Liu Y, Zhou T T, Wang Q, Li Y S. Recent advances in layered double hydroxides (LDHs) as two-dimensional membrane materials for gas and liquid separations. Journal of Membrane Science, 2018, 567: 89–103
9. Wang X R, Chi C L, Zhang K, Qian Y H, Gupta K M, Kang Z X, Jiang J W, Zhao D. Reversed thermo-switchable molecular sieving membranes composed of two-dimensional metal-organic nanosheets for gas separation. Nature Communications, 2017, 8: 14460
10. Wang Y, Li J P, Yang Q Y, Zhong C L. Two-dimensional covalent triazine framework membrane for helium separation and hydrogen purification. ACS Applied Materials & Interfaces, 2016, 8(13): 8694–8701
11. Zhong Z X, Yao J F, Chen R Z, Low Z X, He M, Liu J Z, Wang H T. Oriented two-dimensional zeolitic imidazolate framework-L membranes and their gas permeation properties. Journal of Materials Chemistry. A, Materials for Energy and Sustainability, 2015, 3(30): 15715–15722
12. Shen J, Liu G P, Huang K, Jin W Q, Lee K R, Xu N P. Membranes with fast and selective gas-transport channels of laminar graphene oxide for efficient $CO_2$ capture. Angewandte Chemie International Edition, 2015, 54(2): 578–582
13. Chen L, Shi G S, Shen J, Peng B Q, Zhang B W, Wang Y Z, Bian F G, Wang J J, Li D Y, Qian Z, et al. Ion sieving in graphene oxide membranes via cationic control of interlayer spacing. Nature, 2017, 550(7676): 380–383
14. Zhang M C, Guan K C, Ji Y F, Liu G P, Jin W Q, Xu N P. Controllable ion transport by surface-charged graphene oxide membrane. Nature Communications, 2019, 10(1): 1253
15. Hu R R, Zhang R J, He Y J, Zhao G K, Zhu H W. Graphene oxide-

in-polymer nanofiltration membranes with enhanced permeability by interfacial polymerization. Journal of Membrane Science, 2018, 564: 813–819
16. Li Y, Yuan S, Xia Y, Zhao W, Easton C D, Selomulya C, Zhang X W. Mild annealing reduced graphene oxide membrane for nanofiltration. Journal of Membrane Science, 2020, 601: 117900
17. Liang B, Zhan W, Qi G G, Lin S S, Nan Q, Liu Y X, Cao B, Pan K. High performance graphene oxide/polyacrylonitrile composite pervaporation membranes for desalination applications. Journal of Materials Chemistry. A, Materials for Energy and Sustainability, 2015, 3(9): 5140–5147
18. Yan Y G, Wang W S, Li W, Loh K P, Zhang J. A graphene-like membrane with an ultrahigh water flux for desalination. Nanoscale, 2017, 9: 18951
19. Zhang M C, Mao Y Y, Liu G Z, Liu G P, Fan Y Q, Jin W Q. Molecular bridges stabilize graphene oxide membranes in water. Angewandte Chemie International Edition, 2020, 59(4): 1689–1695
20. Zhang M C, Sun J J, Mao Y Y, Liu G P, Jin W Q. Effect of substrate on formation and nanofiltration performance of graphene oxide membranes. Journal of Membrane Science, 2019, 574: 196–204
21. Liu Y C, Zhu M, Chen M Y, Ma L L, Yang B, Li L L, Tu W W. A polydopamine-modified reduced graphene oxide (RGO)/MOFs nanocomposite with fast rejection capacity for organic dye. Chemical Engineering Journal, 2019, 359: 47–57
22. Cheng P, Chen Y, Gu Y H, Yan X, Lang W Z. Hybrid 2D $WS_2$/GO nanofiltration membranes for finely molecular sieving. Journal of Membrane Science, 2019, 591: 117308
23. Wei S C, Xie Y, Xing Y D, Wang L C, Ye H Q, Xiong X, Wang S, Han K. Two-dimensional graphene oxide/MXene composite lamellar membranes for efficient solvent permeation and molecular separation. Journal of Membrane Science, 2019, 582: 414–422
24. Zhang X K, Li H, Wang J, Peng D L, Liu J D, Zhang Y T. *In-situ* grown covalent organic framework nanosheets on graphene for membrane-based dye/salt separation. Journal of Membrane Science, 2019, 581: 321–330
25. Peng Y, Yao R, Yang W S. A poly(amidoamine) nanoparticle cross-linked two-dimensional metal-organic framework nanosheet membrane for water purification. Chemical Communications, 2019, 55: 3935
26. Liang F, Liu Q, Zhao J, Guan K C, Mao Y Y, Liu G P, Gu X H, Jin W Q. Ultrafast water-selective permeation through graphene oxide membrane with water transport promoters. AIChE Journal. American Institute of Chemical Engineers, 2019, 66(2): e16812
27. Zhao D, Zhao J, Ji Y F, Liu G P, Liu S M, Jin W Q. Facilitated water-selective permeation via PEGylation of graphene oxide membrane. Journal of Membrane Science, 2018, 567: 311–320
28. Huang K, Liu G P, Lou Y Y, Dong Z Y, Shen J, Jin W Q. A graphene oxide membrane with highly selective molecular separation of aqueous organic solution. Angewandte Chemie International Edition, 2014, 53(27): 6929–6932
29. Kim H W, Yoon H W, Yoon S M, Yoo B M, Ahn B K, Cho Y H, Shin H J, Yang H, Paik U, Kwon S, et al. Selective gas transport through few-layered graphene and graphene oxide membranes. Science, 2013, 342(6154): 91–95
30. Naguib M, Kurtoglu M, Presser V, Lu J, Niu J J, Heon M, Hultman L, Gogotsi Y, Barsoum M W. Two-dimensional nanocrystals produced by exfoliation of $Ti_3AlC_2$. Advanced Materials, 2011, 23 (37): 4248–4253
31. Naguib M, Mochalin V N, Barsoum M W, Gogotsi Y. 25th anniversary article: MXenes: a new family of two-dimensional materials. Advanced Materials, 2014, 26(7): 992–1005
32. Naguib M, Mashtalir O, Carle J, Presser V, Lu J, Hultman L, Gogotsi Y, Barsoum M W. Two-dimensional transition metal carbides. ACS Nano, 2012, 6(2): 1322–1331
33. Anasori B, Lukatskaya M R, Gogotsi Y. 2D metal carbides and nitrides (MXenes) for energy storage. Nature Reviews. Materials, 2017, 2(2): 16098
34. Mashtalir O, Naguib M, Mochalin V N, Dall'Agnese Y, Heon M, Barsoum M W, Gogotsi Y. Intercalation and delamination of layered carbides and carbonitrides. Nature Communications, 2013, 4: 1716
35. Gogotsi Y, Anasori B. The rise of MXenes. ACS Nano, 2019, 13 (8): 8491–8494
36. Hantanasirisakul K, Alhabeb M, Lipatov A, Maleski K, Anasori B, Salles P, Ieosakulrat C, Pakawatpanurut P, Sinitskii A, May S J, et al. Effects of synthesis and processing on optoelectronic properties of titanium carbonitride MXene. Chemistry of Materials, 2019, 31(8): 2941–2951
37. Khazaei M, Arai M, Sasaki T, Chung C Y, Venkataramanan N S, Estili M, Sakka Y, Kawazoe Y. Novel electronic and magnetic properties of two-dimensional transition metal carbides and nitrides. Advanced Functional Materials, 2013, 23(17): 2185–2192
38. Hemanth N R, Balasubramanian K. Recent advances in 2D MXenes for enhanced cation intercalation in energy harvesting applications: a review. Chemical Engineering Journal, 2019, 392: 123678
39. Szuplewska A, Kulpinska D, Dybko A, Chudy M, Jastrzebska A M, Olszyna A, Brzozka Z. Future applications of MXenes in biotechnology, nanomedicine, and sensors. Trends in Biotechnology, 2020, 38(3): 264–279
40. Sinha A, Dhanjai, Zhao H M, Huang Y J, Lu X B, Chen J P, Jain R. MXene: an emerging material for sensing and biosensing. Trends in Analytical Chemistry, 2018, 105: 424–435
41. Guo Z L, Zhou J, Zhu L G, Sun Z M. MXene: a promising photocatalyst for water splitting. Journal of Materials Chemistry. A, Materials for Energy and Sustainability, 2016, 4(29): 11446–11452
42. Ihsanullah I. MXenes (two-dimensional metal carbides) as emerging nanomaterials for water purification: progress, challenges and prospects. Chemical Engineering Journal, 2020, 388: 124340
43. Fu L J, Yan Z L, Zhao Q H, Yang H M. Novel 2D nanosheets with potential applications in heavy metal purification: a review. Advanced Materials Interfaces, 2018, 5(23): 1801094
44. Huang X W, Wu P Y. A facile, high-yield, and freeze-and-thaw-assisted approach to fabricate MXene with plentiful wrinkles and its application in on-chip micro-supercapacitors. Advanced Functional Materials, 2020, 30(12): 1910048
45. Ren C E, Hatzell K B, Alhabeb M, Ling Z, Mahmoud K A, Gogotsi

Y. Charge- and size-selective ion sieving through $Ti_3C_2T_x$ MXene membranes. Journal of Physical Chemistry Letters, 2015, 6(20): 4026–4031

46. Ding L, Wei Y Y, Wang Y J, Chen H B, Caro J, Wang H H. A two-dimensional lamellar membrane: MXene nanosheet stacks. Angewandte Chemie International Edition, 2017, 56(7): 1825–1829
47. Ding L, Wei Y Y, Li L B, Zhang T, Wang H H, Xue J, Ding L X, Wang S Q, Caro J, Gogotsi Y. MXene molecular sieving membranes for highly efficient gas separation. Nature Communications, 2018, 9(1): 155
48. Li Z K, Liu Y C, Li L B, Wei Y Y, Caro J, Wang H H. Ultra-thin titanium carbide (MXene) sheet membranes for high-efficient oil/water emulsions separation. Journal of Membrane Science, 2019, 592: 117361
49. Shen J, Liu G Z, Ji Y F, Liu Q, Cheng L, Guan K C, Zhang M C, Liu G P, Xiong J, Yang J, et al. 2D MXene nanofilms with tunable gas transport channels. Advanced Functional Materials, 2018, 28 (31): 1801511
50. Feng X F, Yu Z X, Long R X, Sun Y X, Wang M, Li X H, Zeng G Y. Polydopamine intimate contacted two-dimensional/two-dimensional ultrathin nylon basement membrane supported RGO/PDA/MXene composite material for oil-water separation and dye removal. Separation and Purification Technology, 2020, 247: 116945
51. Saththasivam J, Wang K, Yiming W, Liu Z Y, Mahmoud K A. A flexible $Ti_3C_2T_x$ (MXene)/paper membrane for efficient oil/water separation. RSC Advances, 2016, 9(29): 16296–16304
52. Zhang H J, Wang Z H, Shen Y Q, Mu P, Wang Q T, Li J. Ultrathin 2D $Ti_3C_2T_x$ MXene membrane for effective separation of oil-in-water emulsions in acidic, alkaline, and salty environment. Journal of Colloid and Interface Science, 2020, 561: 861–869
53. Sun Y Q, Li S L, Zhuang Y X, Liu G Z, Xing W H, Jing W Q. Adjustable interlayer spacing of ultrathin MXene-derived membranes for ion rejection. Journal of Membrane Science, 2019, 591: 117350
54. Wu X L, Cui X L, Wu W J, Wang J T, Li Y F, Jiang Z Y. Elucidating ultrafast molecular permeation through well-defined 2D nanochannels of lamellar membranes. Angewandte Chemie International Edition, 2019, 58(51): 18524–18529
55. Ding L, Xiao D, Lu Z, Deng J J, Wei Y Y, Caro J, Wang H H. Oppositely charged $Ti_3C_2T_x$ MXene membranes with 2D nanofluidic channels for osmotic energy harvesting. Angewandte Chemie International Edition, 2020, 59(22): 8720–8726
56. Li J, Li X, Van der Bruggen B. MXene based membrane for molecular separation. Environmental Science. Nano, 2020, 7(5): 1289–1304
57. Lu Z, Wei Y Y, Deng J J, Ding L, Li Z K, Wang H H. Self-crosslinked MXene ($Ti_3C_2T_x$) membranes with good antiswelling property for monovalent metal ion exclusion. ACS Nano, 2019, 13 (9): 10535–10544
58. Xing Y D, Akonkwa G, Liu Z, Ye H Q, Han K. Crumpled two-dimensional $Ti_3C_2T_x$ MXene lamellar membranes for solvent permeation and separation. ACS Applied Nano Materials, 2020, 3 (2): 1526–1534
59. Pandey R P, Rasool K, Madhavan V E, Aïssa B, Gogotsi Y, Mahmoud K A. Ultrahigh-flux and fouling-resistant membranes based on layered silver/MXene ($Ti_3C_2T_x$) nanosheets. Journal of Materials Chemistry. A, Materials for Energy and Sustainability, 2018, 6(8): 3522–3533
60. Shamsabadi A A, Isfahani A P, Salestan S K, Rahimpour A, Ghalei B, Sivaniah E, Soroush M. Pushing rubbery polymer membranes to be economic for $CO_2$ separation: embedment with $Ti_3C_2T_x$ MXene nanosheets. ACS Applied Materials & Interfaces, 2020, 12(3): 3984–3992
61. Hao L, Zhang H Q, Wu X L, Zhang J K, Wang J T, Li Y F. Novel thin-film nanocomposite membranes filled with multi-functional $Ti_3C_2T_x$ nanosheets for task-specific solvent transport. Composites. Part A, Applied Science and Manufacturing, 2017, 100: 139–149
62. Xu Z, Sun Y Q, Zhuang Y X, Jing W H, Ye H, Cui Z F. Assembly of 2D MXene nanosheets and $TiO_2$ nanoparticles for fabricating mesoporous $TiO_2$-MXene membranes. Journal of Membrane Science, 2018, 564: 35–43
63. Liu G Z, Shen J, Liu Q, Liu G P, Xiong J, Yang J, Jin W Q. Ultrathin two-dimensional MXene membrane for pervaporation desalination. Journal of Membrane Science, 2018, 548: 548–558
64. Hong S, Ming F W, Shi Y, Li R Y, Kim I S, Tang C Y, Alshareef H N, Wang P. Two-dimensional $Ti_3C_2T_x$ MXene membranes as nanofluidic osmotic power generators. ACS Nano, 2019, 13(8): 8917–8925
65. Zhang Z, Yang S, Zhang P P, Zhang J, Chen G B, Feng X L. Mechanically strong MXene/Kevlar nanofiber composite membranes as high-performance nanofluidic osmotic power generators. Nature Communications, 2019, 10(1): 2920
66. Lao J C, Lv R J, Gao J, Wang A X, Wu J S, Luo J Y. Aqueous stable $Ti_3C_2$ MXene membrane with fast and photo-switchable nanofluidic transport. ACS Nano, 2018, 12(12): 12464–12471
67. Ding M M, Xu H, Chen W, Yang G, Kong Q, Ng D, Lin T, Xie Z L. 2D laminar maleic acid-crosslinked MXene membrane with tunable nanochannels for efficient and stable pervaporation desalination. Journal of Membrane Science, 2020, 600: 117871
68. Ding L, Li L B, Liu Y C, Wu Y, Lu Z, Deng J J, Wei Y Y, Caro J, Wang H H. Effective ion sieving with $Ti_3C_2T_x$ MXene membranes for production of drinking water from seawater. Nature Sustainability, 2020, 3: 296–302
69. Li L B, Zhang T, Duan Y F, Wei Y Y, Dong C J, Ding L, Qiao Z W, Wang H H. Selective gas diffusion in twodimensional MXene lamellar membranes: insights from molecular dynamics simulations. Journal of Materials Chemistry. A, Materials for Energy and Sustainability, 2018, 6(25): 11734–11742
70. Fan Y Y, Wei L Y, Meng X X, Zhang W M, Yang N T, Jin Y, Wang X B, Zhao M W, Liu S M. An unprecedented high-temperature-tolerance 2D laminar MXene membrane for ultrafast hydrogen sieving. Journal of Membrane Science, 2019, 569: 117–123
71. Jin Y, Fan Y Y, Meng X X, Zhang W M, Meng B, Yang N T, Liu S M. Theoretical and experimental insights into the mechanism for gas separation through nanochannels in 2D Laminar MXene membranes. Processes (Basel, Switzerland), 2019, 7(10): 751
72. Liu G Z, Cheng L, Chen G N, Liang F, Liu G P, Jin W Q. Pebax-based membrane filled with two-dimensional MXene nanosheets

for efficient $CO_2$ capture. Chemistry, an Asian Journal, 2020, 15 (15): 2364–2070

73. Wu Y, Ding L, Lu Z, Deng J J, Wei Y Y. Two-dimensional MXene membrane for ethanol dehydration. Journal of Membrane Science, 2019, 590: 117300
74. Li S S, Dai J, Geng X, Li J D, Li P, Lei J D, Wang L Y, He J. Highly selective sodium alginate mixed-matrix membrane incorporating multi-layered MXene for ethanol dehydration. Separation and Purification Technology, 2020, 235: 116206
75. Liu G Z, Shen J, Ji Y F, Liu Q, Liu G P, Yang J, Jin W Q. Two-dimensional $Ti_2CT_x$ MXene membranes with integrated and ordered nanochannels for efficient solvent dehydration. Journal of Materials Chemistry. A, Materials for Energy and Sustainability, 2019, 7(19): 12095–12104
76. Xu Z, Liu G Z, Ye H, Jin W Q, Cui Z F. Two-dimensional MXene incorporated chitosan mixed-matrix membranes for efficient solvent dehydration. Journal of Membrane Science, 2018, 563: 625–632
77. Liu G Z, Liu S, Ma K, Wang H Y, Wang X Y, Liu G P, Jin W Q. Polyelectrolyte functionalized $Ti_2CT_x$ MXene membranes for pervaporation dehydration of isopropanol/water mixtures. Industrial & Engineering Chemistry Research, 2020, 59(10): 4732–4741
78. Kang K M, Kim D W, Ren C E, Cho K M, Kim S J, Choi J H, Nam Y T, Gogotsi Y, Jung H T. Selective molecular separation on $Ti_3C_2T_x$-graphene oxide membranes during pressure-driven filtration: comparison with graphene oxide and MXenes. ACS Applied Materials & Interfaces, 2017, 9(51): 44687–44694
79. Lin C, Zhang W K, Wang L, Wang Z G, Zhao W, Duan W H, Zhao Z G, Liu B, Jin J. A few-layered $Ti_3C_2$ nanosheet/glass fiber composite separator as a lithium polysulphide reservoir for high-performance lithiumsulfur batteries. Journal of Materials Chemistry. A, Materials for Energy and Sustainability, 2016, 4(16): 5993–5998
80. Zhang S Y, Liao S Y, Qi F Y, Liu R T, Xiao T H, Hu J Q, Li K X, Wang R B, Min Y G. Direct deposition of two-dimensional MXene nanosheets on commercially available filter for fast and efficient dye removal. Journal of Hazardous Materials, 2020, 384: 121367
81. Han R L, Ma X F, Xie Y L, Teng D, Zhang S H. Preparation of a new 2D MXene/PES composite membrane with excellent hydrophilicity and high flux. RSC Advances, 2017, 7: 56204–56210
82. Sun Y Q, Xu Z, Zhuang Y X, Liu G Z, Jin W Q, Liu G P, Jing W H. Tunable dextran retention of MXene-$TiO_2$ mesoporous membranes by adjusting the 2D MXene content. 2D Materials, 2018, 5(4): 045003
83. Gao X, Li Z K, Xue J, Qian Y, Zhang L Z, Caro J, Wang H H. Titanium carbide $Ti_3C_2T_x$ (MXene) enhanced PAN nanofiber membrane for air purification. Journal of Membrane Science, 2019, 586: 162–169
84. Wu X L, Hao L, Zhang J K, Zhang X, Wang J T, Liu J D. Polymer-$Ti_3C_2T_x$ composite membranes to overcome the trade-off in solvent resistant nanofiltration for alcohol-based system. Journal of Membrane Science, 2016, 515: 175–188
85. Han R L, Xie Y L, Ma X F. Crosslinked P84 copolyimide/MXene mixed matrix membrane with excellent solvent resistance and permselectivity. Chinese Journal of Chemical Engineering, 2019, 27(4): 877–883
86. Sun W, Shah S A, Chen Y, Tan Z, Gao H, Habib T, Radovic M, Green M J. Electrochemical etching of $Ti_2AlC$ to $Ti_2CT_x$ (MXene) in low-concentration hydrochloric acid solution. Journal of Materials Chemistry. A, Materials for Energy and Sustainability, 2017, 5(41): 21663–21668
87. Li M, Lu J, Luo K, Li Y B, Chang K K, Chen K, Zhou J, Rosen J, Hultman L, Eklund P, et al. Element replacement approach by reaction with lewis acidic molten salts to synthesize nanolaminated MAX phases and MXenes. Journal of the American Chemical Society, 2019, 141(11): 4730–4737
88. Ling Z, Ren C E, Zhao M Q, Yang J, Giammarco J M, Qiu J S, Barsoum M W, Gogotsi Y. Flexible and conductive MXene films and nanocomposites with high capacitance. Proceedings of the National Academy of Sciences of the United States of America, 2014, 111(47): 16676–16681
89. Ying Y L, Liu Y, Wang X Y, Mao Y Y, Cao W, Hu P, Peng X S. Two-dimensional titanium carbide for efficiently reductive removal of highly toxic chromium(VI) from water. ACS Applied Materials & Interfaces, 2015, 7(3): 1795–1803
90. Huang H B, Ying Y L, Peng X S. Graphene oxide nanosheet: an emerging star material for novel separation membranes. Journal of Materials Chemistry. A, Materials for Energy and Sustainability, 2014, 2(34): 13772–13782
91. Putz K W, Compton O C, Segar C, An Z, Nguyen S T, Brinson L C. Evolution of order during vacuum-assisted self-assembly of graphene oxide paper and associated polymer nanocomposites. ACS Nano, 2011, 5(8): 6601–6609
92. Dikin D A, Stankovich S, Zimney E J, Piner R D, Ruoff R S. Preparation and characterization of graphene oxide paper. Nature, 2007, 448(7152): 457–460
93. Han R Y, Wu P Y. High-performance graphene oxide nanofiltration membrane with continuous nanochannels prepared by the *in situ* oxidation of MXene. Journal of Materials Chemistry. A, Materials for Energy and Sustainability, 2019, 7(11): 6475–6481
94. Cao X P, Jing W H, Xing W H, Fan Y Q, Kong Y, Dong J H. Fabrication of a visible-light response mesoporous $TiO_2$ membrane with superior water permeability via a weak alkaline sol-gel process. Chemical Communications, 2011, 47(12): 3457–3459
95. Zou D, Qiu M H, Chen X F, Fan Y Q. One-step preparation of high-performance bilayer $\alpha$-alumina ultrafiltration membranes via co-sintering process. Journal of Membrane Science, 2017, 524: 141–150
96. Xia C S, Xu Z, Yu J, Sun Y Q, Jing W H. Fabrication of microporous GO-$TiO_2$ membrane via an improved weak alkaline solgel method. Journal of Membrane Science, 2018, 561: 10–18
97. Yu J, Zhang Y, Chen J, Cui L L, Jing W H. Solvothermal-induced assembly of 2D-2D rGO-$TiO_2$ nanocomposite for the construction of nanochannel membrane. Journal of Membrane Science, 2020, 600: 117870
98. Lee Y, Kim S J, Kim Y J, Lim Y, Chae Y, Lee B J, Kim Y T, Han H, Gogotsi Y, Ahn C W. Oxidation-resistant titanium carbide MXene films. Journal of Materials Chemistry. A, Materials for Energy and Sustainability, 2020, 8(2): 573–581
99. Natu V, Hart J L, Sokol M, Chiang H, Taheri M L, Barsoum M W. Edge capping of 2D-MXene sheets with polyanionic salts to

mitigate oxidation in aqueous colloidal suspensions. Angewandte Chemie International Edition, 2019, 58(36): 12655–12660

100. Wang Z H, Li H B, Luo M L, Chen T H, Xia X F, Chen H L, Ma C Y, Guo J, He Z W, Song Y F, et al. MXene photonic devices for near-infrared to mid-infrared ultrashort pulse generation. ACS Applied Nano Materials, 2020, 3(4): 3513–3522

101. Peng J H, Chen X Z, Ong W J, Zhao X J, Li N. Surface and heterointerface engineering of 2D MXenes and their nanocomposites: insights into electro- and photocatalysis. Chem, 2019, 5(1): 18–50

102. Zhang W, Guo Z Y, Huang D Q, Liu Z M, Guo X, Zhong H Q. Synergistic effect of chemo-photothermal therapy using PEGylated graphene oxide. Biomaterials, 2011, 32(33): 8555–8561

103. Chang Z Y, Deng J K, Chandrakumara G G, Yan W Y, Liu J Z. Two-dimensional shape memory graphene oxide. Nature Communications, 2016, 7(1): 11972

104. Kim S, Gupta M K, Lee K Y, Sohn A, Kim T Y, Shin K S, Kim D, Kim S K, Lee K H, Shin H J, et al. Transparent flexible graphene triboelectric nanogenerators. Advanced Materials, 2014, 26(23): 3918–3925